Submonthly Indian Ocean Cooling Events and their Interaction

with Large-Scale Conditions

IAN D. LLOYD *

GABRIEL A. VECCHI

Geophysical Fluid Dynamics Laboratory, National Oceanic and Atmospheric Administration, P. O. Box 308, Princeton, NJ 08542, USA.

_____

Corresponding author address: Ian D. Lloyd, Atmospheric and Oceanic Sciences Program, Princeton

University, 300 Forrestal Road, Sayre Hall, Princeton, NJ 08544, USA.

E-mail: lloyd@princeton.edu

ABSTRACT

The Indian Ocean exhibits strong variability on a number of timescales, including prominent intraseasonal variations in both the atmosphere and ocean. Of particular interest is the south tropical Indian Ocean thermocline ridge, a region located between 12°S - 5°S, which exhibits prominent variability in Sea Surface Temperature (SST) due to dominant winds that raise the thermocline and shoal the mixed layer. In this paper, submonthly (less than 30 day) cooling events in the thermocline ridge region are diagnosed with observations and models, and are related to large-scale conditions in the Indo-Pacific region. Observations from the Tropical Rainfall Measuring Mission (TRMM) Microwave Imager (TMI) satellite were used to identify 16 cooling events in the period 1998-2007, which on average cannot be fully accounted for by air-sea enthalpy fluxes. Analysis of observations and a hierarchy of models, including two coupled global climate models (GFDL CM2.1 and GFDL CM2.4), indicates that ocean dynamical changes are important to the cooling events. Further, it is found that cooling events are preconditioned by large-scale, low-frequency changes in the coupled ocean-atmosphere system. When the thermocline is unusually shallow in the thermocline ridge region, cooling events are more likely to occur and are stronger; these large-scale conditions are more(less) likely during La Niña (El Niño/Indian Ocean Dipole) events. Strong thermocline ridge cooling events are associated with changes in atmospheric convection, which resemble the Madden-Julian oscillation, in both observations and the models.

1. Introduction

The Indian Ocean is a unique region with high mean Sea Surface Temperature (SST) values, strong atmospheric convection, and large variability on intraseasonal to decadal timescales (Schott et al. 2009). Of particular interest here is the Seychelles-Chagos thermocline ridge from 5°S -12°S (see Figure 1.a) which is characterized by strong atmospheric convection and a shallow thermocline, and exhibits large intraseasonal variability in both convection and SST (Harrison and Vecchi 2001; Duvel et al. 2004; Schott et al. 2009; Vialard et al. 2008).

The thermocline ridge is maintained by weak equatorial winds and strong, persistent south-easterly trade winds to the south. These winds drive Ekman divergence and a ridging of the thermocline. In addition, the thermocline ridge region can exhibit strong interannual and decadal variability, driven by local and remote changes in winds (Xie et al. 2002).

The thermocline ridge exhibits both an annual and semi-annual cycle (Hermes and Reason 2008; Yokoi et al. 2008), and is most shallow in boreal winter, when north-westerly near-equatorial monsoonal winds and south-easterly trade winds converge over the Intertropical Convergence Zone and cyclonic wind stress curl (that drives Ekman pumping) is strongest. Oceanic processes, combined with the strong near-equatorial insolation, result in a region with strong vertical temperature stratification with shallow thermocline and mixed layer. Consequently the thermocline ridge is very sensitive to changes in air-sea enthalpy fluxes and intraseasonal SST variability is large (Harrison and Vecchi 2001; Duvel et al. 2004; Saji et al. 2006; Vialard et al. 2008).

The Indian Ocean exhibits substantial interannual variations, including a basin-wide

warming(cooling) in boreal spring after El Niño(La Niña) years in observations and models (Harrison and Larkin 1998; Klein et al. 1999; Song et al. 2007). The Indian Ocean also exhibits zonally asymmetric interannual variability, referred to as the Indian Ocean Dipole (IOD) (Saji et al. 1999; Webster et al. 1999; Murtugudde et al. 2000). In IOD years with positive phase, anomalous easterly winds in the eastern equatorial Indian Ocean lead to Bjerknes-type feedback (Bjerknes 1969), and amplification of an SST anomaly. Associated with El Niño/La Niña and the IOD are variations of surface winds, which can impact the thermal structure of the Indian Ocean, including the thermocline ridge. Changes in the thermocline due to the IOD tend to be north of 10°S, while changes under ENSO are dominant south of 10°S (Rao and Behera 2005; Yu et al. 2005).

The advent of the TRMM Microwave Imager (TMI) observations of SST (Wentz et al. 2000) - which allows for SST estimates even under clouds - has lead to new insights into air-sea interaction processes, even in regions of strong atmospheric convection (Xie et al. 1998; Chelton et al. 2001; Vecchi and Harrison 2002; O'Neill et al. 2003; Vecchi et al. 2004; Saji et al. 2006). These insights include observations of large negative intraseasonal SST anomalies in the thermocline ridge region, primarily in boreal winter. The SST anomalies have significant negative skew, typically last a couple of weeks or less, with magnitudes on the order of 1-3 K or greater, and have been labelled as cooling events (Harrison and Vecchi 2001; Duvel et al. 2004; Saji et al. 2006; Vialard et al. 2008). The precise definition of cooling events used in this paper is outlined in Section 2.*e*. Cooling events predominantly occur in boreal winter when the thermocline is most shallow. We focus on the most extreme events, to characterize the source of negative SST skewness. Warm intraseasonal SST anomalies are also observed but are less extreme, have a smaller negative skew, and are driven by air-sea

3

enthalpy fluxes.

A comprehensive analysis of the underlying physics of cooling events has until now largely been focussed on individual case studies. For instance, diagnosis of two cooling events in January and March 1999 using an Ocean General Circulation Model (OGCM) experiment found the cooling events to be driven by air-sea fluxes (Duvel et al. 2004). Recently, Vialard et al. (2008) explore the observed heat balance for a pair of intraseasonal SST coolings associated with the Madden-Julian Oscillation (MJO) (Madden and Julian 1971, 1994; Zhang 2005) and find that the influence of subsurface processes is smaller than air-sea enthalpy fluxes. However, after a decade of TMI observations, with what confidence can we say that all cooling events are due to air-sea enthalpy fluxes? Is it possible that some cooling events, in addition to air-sea flux exchanges, may in part be caused by vertical entrainment, or Ekman upwelling under increased wind-stress curl? Further, how do cooling events relate to intraseasonal atmospheric variability such as the MJO, and large-scale interannual conditions in the Indo-Pacific region? The potential of these questions for future work has been outlined by Schott et al. (2009): "The role of entrainment needs clarification ... More research with coupled models is necessary to clarify the mechanisms that drive intraseasonal SST variability in the 5°S - 10°S band, and its role in modulating the atmospheric MJO."

The main aim of this paper is to diagnose cooling events in both observations and models, using an increasingly comprehensive ocean heat budget. As a first order approach, a slab layer approximation was used to determine the extent to which observed cooling events can be explained by observational estimates of air-sea enthalpy fluxes. The role of vertical mixing was then estimated using a 1-dimensional mixed layer ocean model (Price et al. 1986). Finally, the role of three-dimensional ocean dynamics was investigated in two global climate

models: 50 years of a control run for the Geophysical Fluid Dynamic Laboratory (GFDL) coupled model CM2.1 (Delworth et al. 2006), and 50 years of a control run for the high resolution, eddy-permitting coupled model GFDL CM2.4 (Thomas Delworth, pers. comm. 2008). In addition, the relation of cooling events to the MJO and phases of the El Niño Southern Oscillation (ENSO) are discussed. Data and Methods are described in Section 2. Results are presented in Section 3, and Section 4 concludes.

2. Data and Methods

a. Observations

SST is taken from the daily TMI-SST OI product produced by Remote Sensing Systems (Gentemann et al. 2004) from January 1998 to December 2007. NCEP Reanalysis-2 data (Kanamitsu et al. 2002) was used for air-sea enthalpy fluxes. Daily surface windstress and wind velocity were obtained from QuikScat satellite data from July 1999 to December 2007 as processed by Cersat (data available at http://cersat.ifremer.fr), with a resolution of 0.25° x 0.25°. The mixed layer depth was taken from Boyer monthly climatology analysis (de Boyer Montégut et al. 2004).

b. Price-Weller-Pinkel (PWP) 1-dimensional mixed layer ocean model

The Price-Weller-Pinkel (PWP) 1-dimensional mixed layer ocean model (Price et al. 1986) was used to test the role of vertical mixing in cooling events. The PWP model has been used to represent the subtropical southern Indian Ocean (Chiodi and Harrison 2007).

In our study, the PWP model was initialized using a temperature-salinity profile for DJF for the Thermocline Ridge Index (TRI), defined as the region 2.5°S - 12.5°S, 50°E - 70°E, from Levitus Climatology analysis (Levitus 1994). During each model time step, shortwave insolation, longwave radiation, and turbulent surface enthalpy fluxes are imposed, and a new density profile is calculated with adjustments for static stability. Wind stresses are then prescribed and used to force the mixed layer momentum balance, and vertical mixing is accounted for with Bulk and Gradient Richardson number mixing. We used a time step of 20 minutes, with a background diffusivity of 2×10^{-5} m^2 s^{-1}. We set the critical Bulk and gradient Richardson numbers to 0.65 and 0.25 respectively. We found the principal results from the PWP model were insensitive to perturbations in the parameter values or the initialization. We used the NCEP Reanalysis-2 for enthalpy and freshwater fluxes, and Quikscat surface winds for momentum fluxes. We forced this configuration of the PWP model with air-sea flux data for each individual cooling event, subtracting a 60-day running mean to correct for a net equatorward inflow of cold water north of 15°S (Godfrey et al. 1995). We then used the resulting outputs for the various events to calculate the composite response.

c. GFDL coupled model CM2.1 control run

We examined cooling events using daily data from the last 50 years of a 300 year control simulation from the Geophysical Fluid Dynamic Laboratory (GFDL) coupled model CM2.1, using invariant 1990's radiative and land use conditions (Delworth et al. 2006; Gnanadesikan et al. 2006; Wittenberg et al. 2006; Stouffer et al. 2006). The atmosphere has a resolution

of 2° x 2.5°, with 24 vertical levels, while the ocean has a resolution of 1° x 1° (with 1/3°
meridional resolution at the equator) and 50 vertical levels. The atmosphere has a finite
volume dynamical core. The model is able to represent many aspects of the mean-state and
interannual variations in the Indian Ocean region (Song et al. 2007).

d. GFDL coupled model CM2.4 control run

In addition to CM2.1, cooling events were examined with daily data from the last 50 years
of a 100 year control simulation from the recently developed coupled model GFDL CM2.4.
1990 radiative and land use conditions were used as for GFDL CM2.1. The atmosphere
has a resolution of 1° x 1°, while the ocean resolution is approximately 0.25° x 0.25°. A
number of features relating to numerical methods and parameterisations have been altered
from CM2.1 (Thomas Delworth, pers. comm. 2008). For the experiment using CM2.4,
three-dimensional subsurface ocean data was only available as monthly averages, while daily
averages were used for two-dimensional surface data.

e. Composite approach

To quantify the tendency of the TMI SST sub 30-day anomaly, SST′, in the thermocline
ridge region towards negative values, the skew of SST′ with standard deviation σ is computed
by:

$$\text{Skew} = \frac{\langle SST'^3 \rangle}{\sigma^3}$$

For the observed period, the TMI SST sub 30-day anomaly in the thermocline ridge region has a statistically significant negative skew of -0.23. We wish to characterize the source of the skewness by focussing on extreme cooling events. To do so, a consistent definition is needed in order to diagnose cooling events and develop a compositing framework. We focus on the TRI, and we define cooling events as days for which the 1-30 day band passed SST anomaly, derived from monthly climatology with daily interpolation, has a negative amplitude in excess of 2.5 standard deviations, as illustrated in Figure 1.b. For discussion of other criteria for cooling events, see Appendix A. The TRI is located in the region where the thermocline is most shallow (see Figure 1.a), and is where cooling events were found to occur with greatest amplitude and frequency, in both observations and the coupled model experiments.

3. Results

a. Nature of cooling events

1) OBSERVATIONS

From January 1998 to December 2007, 16 cooling events were found for the TRI based on the definition in Section 2.*e*. The mean maximum amplitude of the anomaly is -1.4 K for the TRI (Figure 1.c). The composite cooling events are associated with cyclonic and north-westerly wind anomalies which precede the maximum SST cooling, in both observations and the coupled models (Figure 2). The cooling events occur rapidly, over approximately one week or less, while the recovery in general takes longer (Figure 1.c). The maximum

8

net air-sea enthalpy flux out of the ocean occurs approximately three days before the SST anomaly minimum, which suggests that SST changes for cooling events are forced by the atmosphere (Figure 1.d). Composite Outgoing Longwave Radiation (OLR) indicates that strong convection occurs during cooling events, peaking approximately three days before the SST anomaly minimum (Figure 1.e). Both convection and enthalpy fluxes are in quadrature with cooling events, suggesting the possibility of coupled ocean-atmosphere processes connecting all of these.

2) GFDL COUPLED MODELS CM2.1 AND CM2.4

The mean cooling event in CM2.4 has a similar amplitude to that in observations, while the mean event in CM2.1 is slightly weaker than observed, and the mean cooling in PWP is approximately half of the observed value (Figure 3). As with observations, the maximum air-sea enthalpy flux into the ocean occurs approximately three days prior to the SST anomaly minimum. For the two 50 year periods examined in the coupled models, 62 events occurred in CM2.1, and 70 events occurred in CM2.4. The frequency of cooling events in both of the coupled models is comparable to the frequency of events recorded by observations. In addition, CM2.1 and CM2.4 both exhibit negative skewness to the sub-30 day SST anomaly in the TRI, of -0.41 and -0.29 respectively.

b. *Diagnosis of cooling events*

Equation 1 shows the heat budget at the ocean mixed layer characterized by SST, assuming that enthalpy fluxes affect only the mixed layer:

$$\frac{\partial (SST)}{\partial t} = \frac{Q_{sfc}}{\rho c_p h} - \int_{-h}^{0} \underline{V} \cdot \underline{\nabla}(SST) dz + \int_{-h}^{0} (DIFFUSION) dz \qquad (1)$$

Where Q_{sfc} is the net air-sea enthalpy flux, ρ is the density of sea water, taken as 1025 $Kg\ m^{-3}$, c_p is the heat capacity at constant pressure, taken as 3996 $JKg^{-1}K^{-1}$, the mixed layer depth is given by h, and $\underline{V}$ is the advective velocity.

1) SLAB MODEL APPROACH

As an initial approach, we wish to assess the extent to which we can explain the observed and modeled composite SST changes associated with the cooling events via air-sea enthalpy fluxes. Thus, we assume a slab ocean model with fixed mixed layer depth h; in the Boyer climatology (de Boyer Montégut et al. 2004) the mixed layer depth over the TRI is 22 meters for December-February (DJF). Because observations of the mixed layer depth under intense atmospheric convective events indicate that it can deepen substantially and rapidly (Smyth et al. 1996; Vialard et al. 2008), the chosen value may represent a lower bound estimate. From TMI SST, we define the theoretical quantity Q that represents the air-sea enthalpy flux required to explain the observed SST change:

$$Q = \rho c_p h \frac{\partial (SST)}{\partial t} \qquad (2)$$

Figure 4.a shows a comparison of Q with the net air-sea enthalpy flux from NCEP Reanalyis-2 data. Exploration of the individual components of air-sea enthalpy flux indicates that changes in incident shortwave radiation and latent heat are the dominant contributors. The peak value of the theoretical Q quantity for the slab model is significantly larger than

10

the net air-sea flux (-154 W m^{-2} compared to -91 W m^{-2}). The slab model approach implies that for the cooling event composite the NCEP Reanalysis-2 air-sea enthalpy fluxes are not sufficient to explain the observed SST changes. A comparable slab model analysis with Yu-Weller fluxes (Yu and Weller 2007) for the period 1998-2004 yields a similar conclusion (Appendix B). Thus, given current estimates of subseasonal enthalpy fluxes and the mean mixed layer depth, cooling events in the TRI cannot be understood using a "slab ocean" framework.

2) PWP model: Role of vertical mixing

The PWP model allows for another level of complexity to be added to the slab ocean approach; namely, a variable mixed layer and an estimate of vertical diffusion (shown by the final term in Equation 1). When we apply the observational estimates of enthalpy and momentum flux to the PWP model, the resulting SST change is too small to explain observations (Figure 3), and is almost completely due to air-sea enthalpy fluxes (Figure 4.b). This result implies that the inclusion of vertical mixing, as represented in the PWP model with forcing from NCEP Reanalysis-2 fluxes, is insufficient to explain the cooling events. Further, the result suggests that the remaining SST change which was not accounted for by the PWP model may be due to ocean dynamics. The PWP model also indicates that the turbulent mixing alone can lead to a mixed layer deepening of approximately 50% during a cooling event, lending weight to our conjecture that a constant mixed layer depth may underestimate the enthalpy flux required to explain the cooling events.

11

c. Observations and coupled models: Role of Ekman pumping in cooling events

The GFDL coupled models indicate that the air-sea enthalpy fluxes are not sufficient to explain cooling events (Figures 4.c and 4.d). The nature of this result was insensitive to whether a fixed or variable daily mixed layer depth was used. Examination of the meridional cross section in GFDL CM2.1 indicates that for the time evolution of composite cooling events the maximum upwelling in the TRI occurs three days prior to the maximum SST cooling on day 0, and that ocean upwelling is concurrent with a cyclonic wind stress anomaly passing over the TRI (Figure 5). For both coupled model experiments, the meridional cross section of plus 30-day temperature and ocean current anomalies indicate a shallower thermocline, peaking near 8°S (Figures 6.a and 6.b). Associated with the shallow thermocline is a westerly wind anomaly over the TRI (Figures 6.c and 6.d). The anomalous upward current gives some indication that in addition to air-sea enthalpy fluxes, cooling events may be in part due to upwelling of cold water from the subsurface. Further, composite analysis of observation and models shows evidence of Ekman pumping prior to cooling events (Figure 7). In addition to the upwelling at the base of the mixed layer in the TRI region, CM2.1 shows cross-equatorial circulation at the peak latitude of the cooling event.

The following analysis makes use of a one and a half layer ocean approximation in order to compare upwelling in both observations and GFDL CM2.1. Monthly GFDL Ocean Reanalysis data (Zhang et al. 2007) was used for vertically averaged temperature, due to a lack of daily, three-dimensional observational data. Consider the heat budget equation for an infinitesimal volume of water at depth z, with temperature T, vertical velocity w, density ρ, heat capacity c_p, and vertical enthalpy flux $Q(z)$:

$$\frac{\partial T}{\partial t} - \frac{1}{\rho c_p}\frac{\partial Q(z)}{\partial z} = -w\frac{\partial T}{\partial z} + \epsilon \tag{3}$$

$Q(z)$ is a function of depth, representing shortwave penetration below the surface, and the sum of shortwave, longwave, latent heat, and sensible heat at the surface. A residual term for horizontal advection and diffusion is represented by ϵ.

For the purposes of the Ekman upwelling argument the ocean is divided into a slab layer and a sub layer (Figure 8), where the slab layer is at a depth below the mixed layer. To progress further a Reynolds decomposition is used:

$$T = \langle T \rangle + T' \tag{4}$$

$$Q = \langle Q \rangle + Q' \tag{5}$$

$$w = \langle w \rangle + w' \tag{6}$$

Square brackets indicate the mean component, while the anomaly is indicated by a prime. Integrating Equation 3 over the upper slab layer to a depth z = -H gives the following:

$$\int_{-H}^{0}\left(\frac{\partial T'}{\partial t} - \frac{1}{\rho c_p}\frac{\partial Q'}{\partial z}\right)dz = \int_{-H}^{0}\left(-w'\frac{\partial \langle T \rangle}{\partial z} - \langle w \rangle\frac{\partial T'}{\partial z} - w'\frac{\partial T'}{\partial z}\right)dz + \epsilon \tag{7}$$

The second and third terms on the right hand side of Equation 7 are neglected here. The justification is that the terms w' and $\langle w \rangle$ are of approximately equal magnitude for the TRI, while over a depth of $H = 60$ metres, $\frac{\partial T'}{\partial z}$ is approximately an order of magnitude less than $\frac{\partial \langle T \rangle}{\partial z}$. Explicitly, over the 15 day integration period for the TRI, w' and $\langle w \rangle$ are 0.39 m/day and 0.49 m/day respectively (approximately equal magnitude), while the change in T' and $\langle T \rangle$ between 0 and 60 meters is 0.23K and 4.71K respectively (approximately a factor of 20).

13

The advantage of making this simplification is that we can compare results between CM2.1 and observations, because daily temperature anomaly data as a function of depth are not present for the TRI. Using values of H between 50 and 100 metres does not affect the results from this analysis, as long as H is below the mixed layer depth. Finally, integration by parts from the surface to depth H yields:

$$\frac{\partial \bar{T}'}{\partial t} - \frac{Q'_{sfc}}{\rho c_p H} = -w'_{ek}\frac{(\langle T \rangle - \langle T_{-H} \rangle)}{H} + \epsilon \tag{8}$$

Where $\langle T_{-H} \rangle$ is the mean temperature at the base of the sublayer. An overbar denotes vertical average (for instance, $\bar{T}'$ is the vertically averaged temperature anomaly in the slab layer), and w_{ek} is the Ekman upwelling, related to the curl of the wind stress:

$$w_{ek} = -\underline{\nabla} \times \left(\frac{\tau}{\rho f}\right) \tag{9}$$

where f is the Coriolis parameter. Figure 9 shows the result of testing Equation 8 in observations and the GFDL coupled models respectively. For observations, $\bar{T}'$ is approximated as the surface temperature anomaly (not the vertically averaged temperature anomaly of the slab, as required). This is the best approximation given the lack of daily temperature data, but cannot be justified physically. The quantities were averaged over a period of 15 days prior to the cooling event.

For the CM2.1 model (Figure 9.b), the slope is 0.98 ± 0.31 at the 95% confidence level, which is a strong indication that the upper ocean temperature change not due to air-sea enthalpy fluxes may be due to Ekman upwelling from enhanced cyclonic wind stress curl. For observations (Figure 9.a), the slope is 0.51 ± 0.47 at the 95% confidence level. This gives

some indication that Ekman upwelling is important. However, more observations are needed to fully test this, and advances in the Indian Ocean observation network will help provide some of the necessary observations (e.g. CLIVAR-GOOS Indian Ocean Panel and Collaborators 2006; Vialard et al. 2008). From CM2.1, one expects that the SST anomaly is less than $\bar{T}'$; if this is true for observations, then we speculate that if $\bar{T}'$ were used instead of the SST anomaly in observations, then the slope would be closer to unity.

The gradient of the slope in CM2.1 is close to unity, indicating that a large fraction of the temperature anomaly in the slab layer not due to air-sea enthalpy fluxes can be explained by Ekman upwelling.

d. Ocean preconditioning associated with cooling events

If ocean processes are important for cooling events, then there can be an important role for ocean preconditioning in modulating their frequency and intensity. Mean state conditions associated with cooling events in the coupled models indicate that cooling events tend to occur when the thermocline in the Indian Ocean is shallower than normal and the temperature stratification is stronger (Figures 5 and 6). In much the same way that seasonal variations in the thermocline tend to precondition cooling events, an anomalously shallow thermocline would make upwelling more effective due to increased near surface stratification (see Section 3.c), and would enhance the impact of changes in air-sea enthalpy fluxes due to reduced solar insolation and increased latent heat out of the ocean for a shallower mixed layer.

This preconditioning of an anomalously shallow thermocline in the TRI is associated

with La Niña-like conditions (see Figure 10), with warming over the Indo-Pacific warm pool, increased Walker circulation, and increased anomalous westerly surface winds over the Indian Ocean thermocline ridge. Two mechanisms could be responsible for a shallower thermocline in the TRI. Firstly, enhanced cyclonic wind stress curl in the south-eastern Indian Ocean could lead to upwelling Rossby waves, which emerge within the proximity of the TRI after several months (Xie et al. 2002). Secondly, enhanced Walker circulation over the Indo-Pacific region is associated with increased westerly winds over the equatorial Indian Ocean, which would tend to drive a shallower thermocline through Ekman divergence.

e. Relation of cooling events to the Madden-Julian Oscillation (MJO)

Using the cooling event index defined in Section 2.e, we can plot a Hovmoller diagram for OLR averaged over 5°S-12°S (Figure 11.a) for observations. An eastward propogating signal with a phase speed of approximately 5 m s^{-1} is present, which is comparable to that of the MJO (Madden and Julian 1994; Maloney and Hartmann 1998).

The precipitation anomaly associated with this cooling event composite has a maximum of 4 mm day^{-1} approximately three days before the SST anomaly minimum (Figure 12.a). When using an index based on precipitation events of 4 mm day^{-1} or greater, the Hovmoller diagram for OLR contains a weaker signal with propagation not travelling beyond the date line (Figure 11.b).

Comparing cooling event and precipitation event indices shows that cooling events are associated with a stronger MJO signal. Further, when comparing the SST response associated with each of the two indices, it can be seen that the SST anomaly is weaker for precipitation

16

events than for cooling events (Figure 12.b). This raises several questions:

- Strong MJO events induce strong SST variability. Does strong SST variability feed back to the atmosphere and influence the MJO? Strong cooling would act to stabilize the boundary layer, which under certain mechanisms for the MJO could act to aid eastward propagation (Zhang and Anderson 2003).

- In many coupled General Circulation Models (GCM's), the MJO is poorly represented (Lin et al. 2006). If SST feedback is important for the MJO, could the representation of the MJO be improved in coupled GCM's if the SST variability, which is too weak in the Indian Ocean, were to be improved?

- If cooling events are associated with a strong MJO signal, could observation of a cooling event, or strong sub 30-day SST variability in general, improve skill in forecasting temperature and precipitation patterns in the Indo-Pacific region on MJO timescales?

4. Discussion and conclusion

Our diagnosis of Indian Ocean cooling events in observations and the output from two GFDL coupled models indicates that, on average, strong cooling events cannot be accounted for by air-sea enthalpy fluxes alone (though individual events may). A hierarchy of models is used to show that dynamical ocean processes are necessary to explain extreme cooling events in the TRI. Air-sea fluxes account for approximately 50% of the observed composite of the strongest cooling events in observations and GFDL coupled models (Table 1). For weaker cooling events with smaller negative skew, air-sea enthalpy fluxes constitute a greater

17

proportion of the composite cooling (Table 2).

A simple one and a half layer ocean thermodynamic balance indicates that Ekman upwelling may play an important role in the upper ocean heat balance during cooling events. Blooms seen in SeaWIF chlorophyll data also suggest that ocean dynamical processes are present during cooling events (Resplandy et al. 2009), but sustained observations of three-dimensional evolution of the ocean are still required for a more complete picture of the processes behind cooling events. Single column ocean models forced with estimates of enthalpy fluxes were unable to fully explain the composite cooling event (the resulting cooling was too weak). Results from the PWP model indicate that its parameterizations of vertical mixing were not sufficient to account for oceanic processes essential to cooling events using forcing from NCEP Reanalysis-2 data (or Yu-Weller fluxes). This may in part be due to the strong temperature stratification in the region, or the presence of barrier layers at the ocean surface, and in our assessment it underlines the likely importance of three-dimensional ocean dynamics to cooling events. In these one-dimensional models, the air-sea enthalpy fluxes were able to drive only weak cooling events.

Our findings that cooling events involve ocean dynamical processes which contribute to the composite SST response are consistent with results from Vinayachandran and Saji (2008) and Resplandy et al. (2009). However, analysis of cooling events in Duvel et al. (2004) and Vialard et al. (2008) found that for some specific cases, air-sea enthalpy fluxes are sufficient to explain the observed SST changes. For these specific cases, we also find cooling events to be driven by air-sea fluxes. But when considering all sixteen cooling events in the TRI over a ten year period in observations, defined with a 2.5σ threshold, we find that ocean processes are important in explaining the observed SST changes (Table 1).

Observations and the GFDL coupled models also indicate that cooling events have a higher probability of occurring when the local thermocline and mixed layer are shallower, and near-surface thermal stratification is strong. A shallow thermocline tends to be associated with an increased Walker circulation and La Niña conditions. Observational assessment of this large-scale preconditioning will require a longer record of TRMM/TMI type data covering more phases of ENSO. In the GFDL coupled model composites, La Niña conditions exist in the Pacific 5-12 weeks before cooling events occur (Figure 10). The possible link between cooling events, associated shifts in eastward convection, and changes in the phase of ENSO should be investigated further.

We hypothesize that La Niña conditions lead to a preconditioning that favors cooling events, while El Niño or IOD conditions are unfavorable for cooling events. Our conjecture is based on the observation that La Niña conditions, with enhanced Walker circulation and increased equatorial westerly surface winds over the Indian Ocean lead to a shallower thermocline in the TRI which, by making cold subsurface water more readily available to the surface, favors the occurrence of cooling events.

In addition, a deeper thermocline in IOD years would cause less favorable conditions for cooling events. For instance, one possible explanation for the lack of any cooling events in 1998 could be that the strong IOD event in 1997/1998 caused a deep thermocline in the TRI. The relative influence of ENSO and the IOD in preconditioning the TRI, and determining the frequency of cooling events, should be further investigated.

This coupled preconditioning of cooling events, on interannual and other timescales, should be explored in subsequent work - including possible influences of decadal and radiatively forced changes to the Indian Ocean thermal structure. For instance, a negative phase

of the Pacific Decadal Oscillation, associated with a "La Niña" like pattern with increased westerly winds over the thermocline ridge and a shallower thermocline may make cooling events more prominent. In addition, the projections of a weakened Walker circulation, and related IOD-like state in the Indian Ocean, from increases in greenhouse gases (Vecchi et al. 2006; Held and Soden 2006; Vecchi and Soden 2007), suggest the possibility that there may develop a long-term tendency for a reduction in the frequency and intensity of cooling events.

Finally, as strong cooling events were found to be related to MJO-like convective variability, it appears that there may be a role for cooling events in the evolution of the MJO. Future work should investigate the dynamical relationships between these two phenomena: Does intraseasonal SST variability in the thermocline ridge region influence the MJO, or are the oceanic changes largely unimportant to the subsequent evolution of the MJO? Also, does the relationship between cooling events and the MJO arise in part from the characteristic forcing exerted by the MJO, in contrast to that from other types of intraseasonal atmospheric variability?

Continued and expanded efforts to monitor, understand, and represent strong cooling events, and the evolution of the momentum and enthalpy fluxes, as well as the evolution of the oceanic state, will help refine our understanding of the role of fluxes and ocean dynamics in driving cooling events.

course of this work. This report was prepared by Ian Lloyd under award NA17RJ2612 and NA08OAR4320752 from the National Oceanic and Atmospheric Administration, U.S. Department of Commerce. The statements, findings, conclusions, and recommendations are those of the authors and do not necessarily reflect the views of the National Oceanic and Atmospheric Administration, or the U.S. Department of Commerce.

APPENDIX A

The cooling event composite analysis was repeated using a 1.5 - 2.5 standard deviation criteria (Figure 13). The result of these composites showed that weaker cooling events, with smaller negative skew, were driven primarily by air-sea enthalpy fluxes. In addition, ocean preconditioning is not important for these less extreme events (Figure 14). Because we wish to focus on the most extreme events with large negative skew, the paper addresses cooling events with a standard deviation of 2.5 or greater.

Use of a sub-60 day criteria for cooling events does not have any significant impact on the nature of the results, as almost all cooling events are captured by the sub-30 day criteria.

APPENDIX B

To test the validity of the slab model approach using NCEP Reanalysis-2 fluxes, a similar analysis was performed with Yu-Weller fluxes (Yu and Weller 2007) for the period 1998-2004. For a clean comparison, the composite analysis with NCEP Reanalysis-2 data was also repeated for 1998-2004. Yu-Weller fluxes indicate that the discrepancy between the net air-sea enthalpy flux and the theoretical quantity Q is even stronger than for NCEP reanalysis-2 data (Figure 15). This result further supports the argument that air-sea enthalpy fluxes are not sufficient to explain the observed SST changes.

REFERENCES

Bjerknes, J., 1969: Atmospheric teleconnections from the equatorial Pacific. *Mon. Wea. Rev.*, **97**, 163–172.

Chelton, D. B., S. K. Esbensen, M. G. Schlax, N. Thum, and M. H. Freilich, 2001: Observations of coupling between surface wind stress and sea surface temperature in the eastern tropical Pacific. *J. Climate*, **14**, 1479–1498.

Chiodi, A. M. and D. E. Harrison, 2007: Mechanisms of summertime subtropical southern indian ocean sea surface temperature variability: On the importance of humidity anomalies and the meridional advection of water vapor. *J. Climate*, **20**, 48354852.

de Boyer Montégut, C., C. G. Madec, A. S. Fischer, A. Lazar, and D. Iudicone, 2004: Mixed layer depth over the global ocean: An examination of profile data and a profile-based climatology. *J. Geophys. Res.*, **109**, C12 003, doi:10.1029/2004JC002378.

Delworth, T. L., et al., 2006: GFDL's CM2 Global Coupled Climate Models. Part I: Formulation and simulation characteristics. *J. Climate*, **19**, 643–674.

Duvel, J. P., R. Roca, and J. Vialard, 2004: Ocean mixed layer temperature variations induced by intraseasonal convective perturbations over the Indian Ocean. *J. Atmos. Sci.*, **61**, 3056–3082.

Gentemann, C. L., F. J. Wentz, C. A. Mears, and D. K. Smith, 2004: In situ validation

of Tropical Rainfall Measuring Mission microwave sea surface temperatures. *J. Geophys. Res.*, **109**, C04 021, doi:10.1029/2003JC002092.

Gnanadesikan, A., et al., 2006: GFDL's CM2 global coupled climate models - part II: The baseline ocean simulation. *J. Climate*, **19**, 675–697.

Godfrey, J. S., et al., 1995: The role of the Indian Ocean in the global climate system: Recommendations regarding the global ocean observing system. Report of the Ocean Observing System Development Panel, Texas A&M University, 89 pp.

Harrison, D. E. and N. Larkin, 1998: El niño-Southern Oscillation surface temperature and wind anomalies, 1946-1993. *Rev. Geophys.*, **36**, 353–399.

Harrison, D. E. and G. A. Vecchi, 2001: January 1999 Indian Ocean cooling event. *Geophys. Res. Lett.*, **28**, 3717–3720.

Held, I. M. and B. J. Soden, 2006: Robust responses of the hydrological cycle to global warming. *J. Climate*, **19**, 5686–5699.

Hermes, J. C. and C. J. C. Reason, 2008: Annual cycle of the South Indian Ocean (Seychelles-Chagos) thermocline ridge in a regional ocean model. *J. Geophys. Res.*, **113**, C04 035, doi:10.1029/2007JC004363.

Kanamitsu, M., W. Ebisuzaki, J. Woollen, S.-K. Yang, J. J. Hnilo, M. Fiorino, and G. L. Potter, 2002: NCEP-DOE AMIP-II Reanalysis (R-2). *Bull. Amer. Meteor. Soc.*, **83**, 1631–1643.

Klein, S. A., B. J. Soden, and N.-C. Lau, 1999: Remote sea surface temperature variations during ENSO: Evidence for a tropical atmospheric bridge. *J. Climate*, **12**, 917–932.

Levitus, S., 1994: World ocean atlas 1994 cd rom sets. *National Oceanographic Data Center Informal Rep. 13*, 30 pp.

Lin, J.-L., et al., 2006: Tropical intraseasonal variability in 14 IPCC AR4 climate models. part I: Convective signals. *J. Climate*, **19**, 2665–2690.

Madden, R. A. and P. R. Julian, 1971: Detection of a 40-50 Day Oscillation in the Zonal Wind in the Tropical Pacific. *J. Atmos. Sci.*, **28**, 702–708.

Madden, R. A. and P. R. Julian, 1994: Observations of the 40-50 day tropical oscillation: A review. *Mon. Wea. Rev.*, **112**, 814–837.

Maloney, E. D. and D. L. Hartmann, 1998: Frictional moisture convergence in a composite life cycle of the Madden-Julian Oscillation. *J. Climate*, **11**, 2387–2403.

Murtugudde, R., J. P. McCreary Jr., and A. J. Busalacchi, 2000: Oceanic processes associated with anomalous events in the Indian Ocean with relevance to 1997-1998. *J. Geophys. Res.*, **105**, 3295–3306.

O'Neill, L. W., D. B. Chelton, and S. K. Esbensen, 2003: Observations of SST-induced perturbations of the wind stress field over the Southern Ocean on seasonal timescales. *J. Climate*, **16**, 2340–2354.

Price, J. F., R. A. Weller, and R. Pinkel, 1986: Diurnal cycling: Observations and models of

the upper ocean response to diurnal heating, cooling, and wind mixing. *J. Geophys. Res.*, **91**, 8411–8427.

Rao, S. A. and S. K. Behera, 2005: Subsurface influence on SST in the Tropical Indian Ocean: Structure and Interannual Variability. *Dynamics of Atmosphere and Ocean*, **39**, 103–135.

Resplandy, L., J. Vialard, M. Lévy, O. Aumont, and Y. Dandonneau, 2009: Seasonal and intraseasonal biogeochemical variability in the thermocline ridge of the Indian Ocean. *J. Geophys. Res., in press*, doi:10.1029/2008JC005246.

Saji, N. H., B. N. Goswami, P. N. Vinayachandran, and T. Yamagata, 1999: A dipole mode in the tropical Indian Ocean. *Nature*, **401**, 360–363.

Saji, N. H., S.-P. Xie, and C. Y. Tam, 2006: Satellite observations of intense intraseasonal cooling events in the tropical south Indian Ocean. *Geophys. Res. Lett.*, **33**, L14 704, doi: 10.1029/2006GL026525.

Schott, F. A., S.-P. Xie, and J. McCreary, 2009: Indian Ocean circulation and climate variability. *Rev. Geophys.*, **47**, RG1002, doi:10.1029/2007RG000245.

Smyth, W. D., D. Hebert, and J. N. Moum, 1996: Local ocean response to a multiphase westerly wind burst: 2. thermal and freshwater responses. *J. Geophys. Res.*, **101**, 22 513–22 533.

Song, Q., G. A. Vecchi, and A. J. Rosati, 2007: Indian Ocean variability in the GFDL Coupled Climate Model. *J. Climate*, **20**, 2895–2916.

Stouffer, R. J., et al., 2006: GFDL's CM2 global coupled climate models. part IV: Idealized climate response. *J. Climate*, **19**, 723–740.

CLIVAR-GOOS Indian Ocean Panel and Collaborators, 2006: Understanding the role of the Indian Ocean in the climate system - implementation plan for sustained observations. Tech. rep., International CLIVAR Project Office, 76 pp., Southampton, UK. ICPO Publication Series, 100.

Vecchi, G. A. and D. E. Harrison, 2002: Monsoon breaks and subseasonal sea surface temperature variability in the Bay of Bengal. *J. Climate*, **15**, 1485–1493.

Vecchi, G. A., B. Soden, A. Wittenberg, I. Held, A. Leetmaa, and M. Harrison, 2006: Weakening of tropical Pacific atmospheric circulation due to anthropogenic forcing. *Nature*, **441**, doi:10.1038/nature04744.

Vecchi, G. A. and B. J. Soden, 2007: Global warming and the weakening of the tropical circulation. *J. Climate*, **20**, 4316–4340.

Vecchi, G. A., S.-P. Xie, and A. S. Fischer, 2004: Ocean-atmosphere covariability in the Western Arabian Sea. *J. Climate*, **17**, 1213–1224.

Vialard, J., G. Foltz, M. McPhaden, J. P. Duvel, and C. de Boyer Montégut, 2008: Strong Indian Ocean cooling associated with the Madden-Julian oscillation in late 2007 and early 2008. *Geophys. Res. Lett.*, **35**, L19 608, doi:10.1029/2008GL035238.

Vinayachandran, P. N. and N. H. Saji, 2008: Mechanisms of south Indian Ocean intraseasonal cooling. *Geophys. Res. Lett.*, **35**, L23 607, doi:10.1029/2008GL035733.

Webster, P. J., A. M. Moore, J. P. Loschnigg, and R. R. Leben, 1999: Coupled oceanic-atmospheric dynamics in the Indian Ocean during 1997-98. *Nature*, **401**, 356–360.

Wentz, F. J., C. Gentemann, D. Smith, and D. Chelton, 2000: Satellite measurements of sea surface temperature through clouds. *Science*, **288**, 847–850.

Wittenberg, A. T., A. Rosati, N.-C. Lau, and J. J. Ploshay, 2006: GFDL's CM2 global coupled climate models. part III: Tropical Pacific climate and ENSO. *J. Climate*, **19**, 698–722.

Xie, S.-P., H. Annamalai, F. A. Schott, and J. P. McCreary Jr., 2002: Structure and mechanisms of south Indian Ocean climate variability. *J. Climate*, **15**, 864–878.

Xie, S.-P., M. Ishiwatari, H. Hashizume, and K. Takeuchi, 1998: Coupled ocean-atmospheric waves on the equatorial front. *Geophys. Res. Lett.*, **25**, 3863–3866.

Yokoi, T., T. Tozuka, and T. Yamagata, 2008: Seasonal variation of the Seychelles Dome. *J. Climate*, **21**, 3740–3754.

Yu, L. and R. A. Weller, 2007: Objectively Analyzed air-Sea Heat Fluxes for the Global Ice-Free Oceans (1981-2005). *Bull. Amer. Meteor. Soc.*, **88**, 527539.

Yu, W., W. B. Xiang, L. Liu, and N. Liu, 2005: Understanding the origins of interannual thermocline variations in the tropical Indian Ocean. *Geophys. Res. Lett.*, **32**, L24 706, doi:10.1029/2005GL024327.

Zhang, C., 2005: Madden-Julian Oscillation. *Rev. Geophys.*, **43**, RG2003, doi:10.1029/2004RG000158.

Zhang, C. and S. P. Anderson, 2003: Sensitivity of intraseasonal perturbations in SST to the structure of the MJO. *J. Atmos. Sci.*, **60**, 2196–2207.

Zhang, S., M. J. Harrison, A. Rosati, and A. Wittenberg, 2007: System design and evaluation of coupled ensemble data assimilation for global oceanic climate studies. *Mon. Wea. Rev.*, **135**, 3541–3564.

List of Tables

TABLE 1. Table of Q-HF heat budget analysis, showing the percentage contribution to composite SST changes due to vertical processes and air-sea enthalpy fluxes over 15 days prior to the cooling event maximum. Results for the PWP model are excluded, as cooling events are too weak compared to observations. The threshold criteria for cooling events is 2.5σ.

Quantity (J/m^2)	OBS	CM2.1	CM2.4
Vertical processes: $\int_{-15}^{0}(Q-HF).dt$	45.1%	50.1%	45.0%
Air-sea fluxes: $\int_{-15}^{0}(HF).dt$	54.9%	49.9%	55.0%

TABLE 2. Same as Table 1, but with a threshold of $(1.5 - 2.5)\sigma$.

Quantity (J/m^2)	OBS	CM2.1	CM2.4
Vertical processes: $\int_{-15}^{0} (Q - HF).dt$	25.1%	15.3%	27.9%
Air-sea fluxes: $\int_{-15}^{0} (HF).dt$	74.9%	84.7%	72.1%

List of Figures

3   Sub 30-day composite SST anomaly (K) for observations, the PWP model, and GFDL coupled models CM2.1 and CM2.4, averaged over the TRI.   39

4   a) Observations: Comparison of NCEP Reanalysis-2 air-sea enthalpy fluxes (black) with theoretical flux $Q = \rho c_p h \frac{\partial(SST)}{\partial t}$, in W m^{-2}, calculated from TMI-SST data (blue). The mixed layer depth is taken as 22m from Boyer climatology. Individual components of the air-sea enthalpy fluxes are shown in color. b) PWP model: NCEP Reanal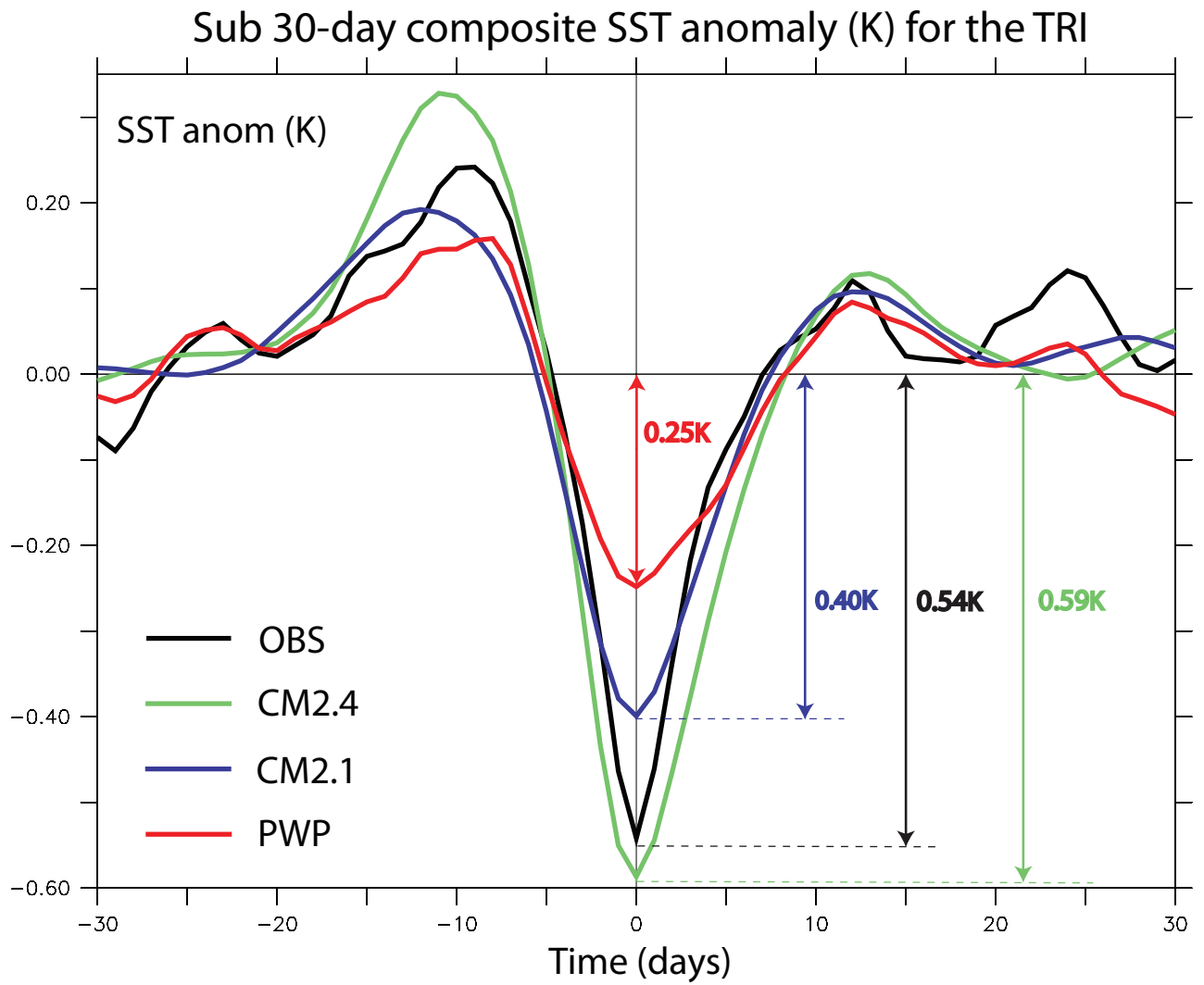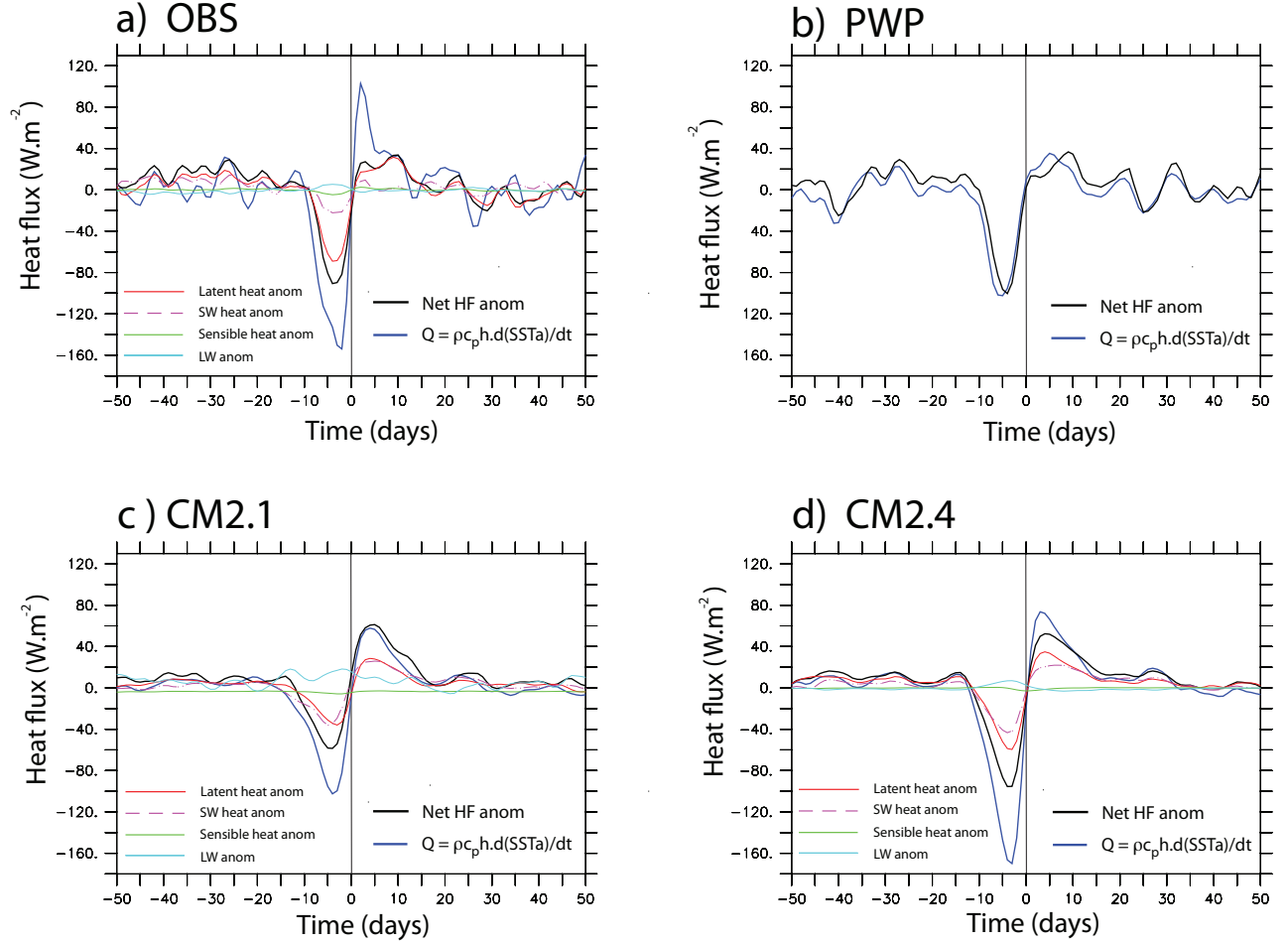ysis-2 air-sea enthalpy flux (black) versus the Q flux (blue) derived from the PWP composite response. c) and d) are the same as for a), but for GFDL CM2.1 and GFDL CM2.4 models respectively.   40

5   Left and Center: Meridional cross section (55°E-65°E average) for the TRI composite on days -3, 0, and +3, for GFDL CM2.1. Shading indicates temperature anomaly (K) (left column) and sub-30 day temperature anomaly (center column); contours indicate mean temperature (K), with the red contour showing the 20 K isotherm; arrows indicate current anomalies (m s^{-1}) (left column) and sub-30 day current anomalies (center column). The vertical scale for current anomalies is magnified by a factor of 10,000. Right: Wind stress anomalies (10^{-2} Pa) averaged over 55°E-65°E for days -3, 0, and +3.   41

FIG. 1. a) Shaded: Levitus Climatology analysis for near-surface ocean temperature (0m-40m average) minus sub-surface ocean temperature (70m-110m average), for JFM (in K). High values indicate strong temperature stratification. The boxed region represents the Thermocline Ridge Index (TRI), defined as 50°E - 70°E, 2.5°S - 12.5°S. Contours represent low OLR (W m^{-2}) for JFM. b) 1-30 day band passed SST anomaly (K), based on TMI SST observations for the TRI. Cooling events are represented by points at which the sub 30-day SST anomaly crosses the dashed 2.5σ line. c) SST anomaly (K) for 16 cooling events, from Jan 1998 to Dec 2007, for the TRI. The time scale (in days) is set so day 0 represents the minimum SST anomaly for each cooling event. The red line represents the composite of events. d) Air-sea enthalpy flux anomaly (W m^{-2}) for 16 cooling events for the TRI, from NCEP Reanalysis-2 data (positive values indicate net air-sea enthalpy flux into the ocean). e) Outgoing Longwave Radiation (OLR) (W m^{-2}) for 16 cooling events for the TRI, from NCEP Reanalysis-2 data.

38
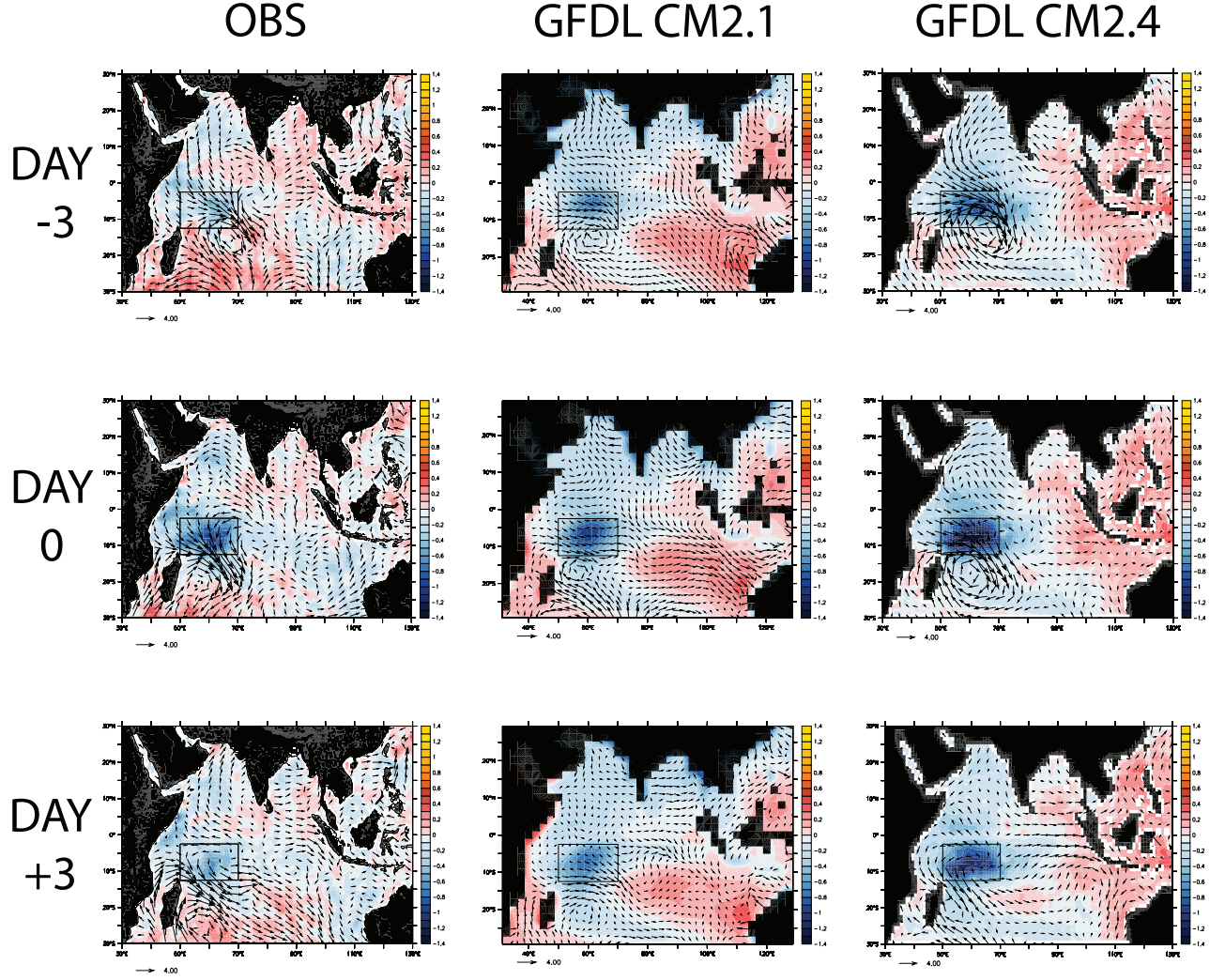
F<small>IG</small>. 2. Cooling event composite for the TRI, on days -3, 0, and +3, for observations, GFDL CM2.1, and GFDL CM2.4. SST anomaly (K) is shaded. Vectors represent surface wind anomalies (m s^{-1}), with QuikScat winds used for observations. The maximum cooling of 1.4 K over the TRI on day 0 in observations is associated with anomalous north-westerly winds.

FIG. 3. Sub 30-day composite SST anomaly (K) for observations, the PWP model, and GFDL coupled models CM2.1 and CM2.4, averaged over the TRI.

FIG. 4. a) Observations: Comparison of NCEP Reanalysis-2 air-sea enthalpy fluxes (black) with theoretical flux $Q = \rho c_p h \frac{\partial(SST)}{\partial t}$, in W m^{-2}, calculated from TMI-SST data (blue). The mixed layer depth is taken as 22m from Boyer climatology. Individual components of the air-sea enthalpy fluxes are shown in color. b) PWP model: NCEP Reanalysis-2 air-sea enthalpy flux (black) versus the Q flux (blue) derived from the PWP composite response. c) and d) are the same as for a), but for GFDL CM2.1 and GFDL CM2.4 models respectively.

GFDL CM2.1
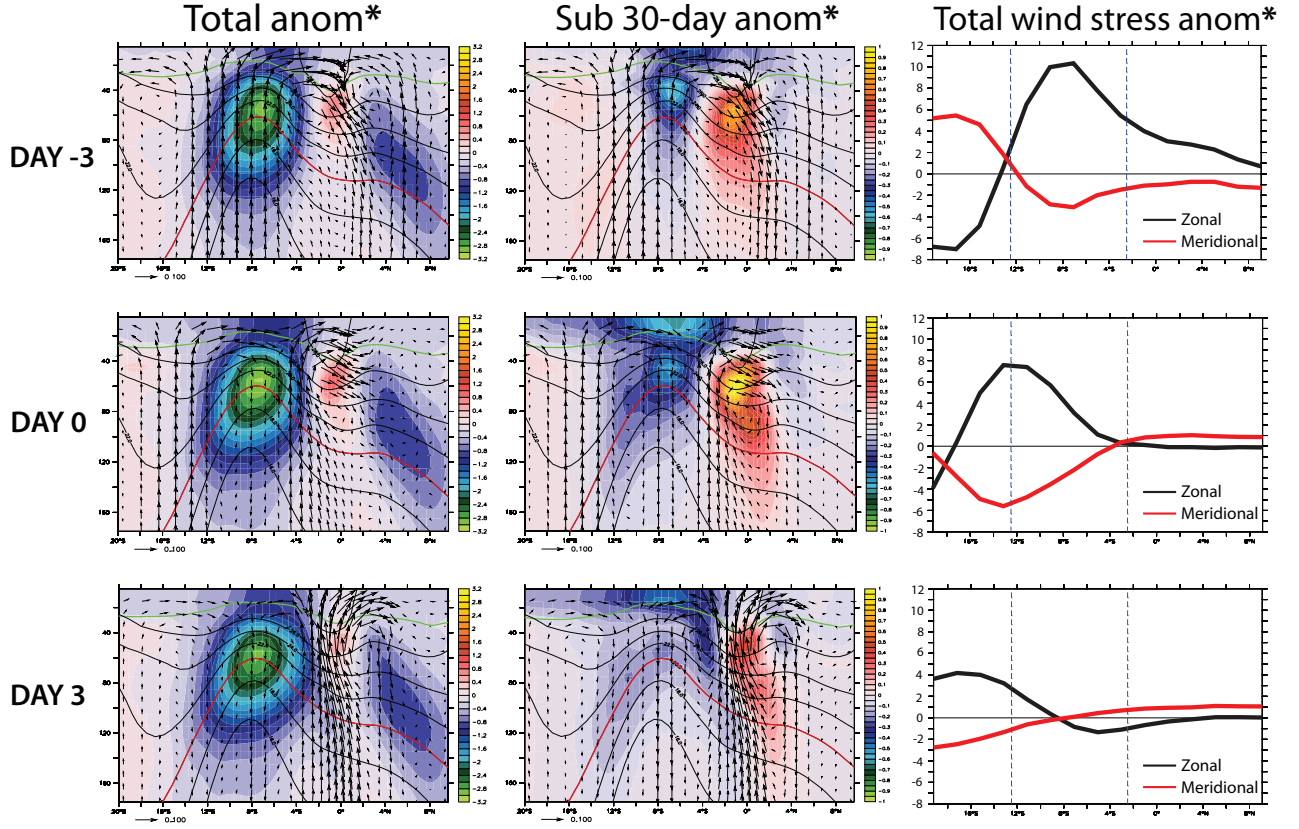
*Left and center: Temperature anomaly (shaded, K); temperature (contour, K); current anomaly (m s^{-1}). Right: Total wind stress anomaly (10^{-2}Pa)

FIG. 5. Left and Center: Meridional cross section (55°E-65°E average) for the TRI composite on days -3, 0, and +3, for GFDL CM2.1. Shading indicates temperature anomaly (K) (left column) and sub-30 day temperature anomaly (center column); contours indicate mean temperature (K), with the red contour showing the 20 K isotherm; arrows indicate current anomalies (m s^{-1}) (left column) and sub-30 day current anomalies (center column). The vertical scale for current anomalies is magnified by a factor of 10,000. Right: Wind stress anomalies (10^{-2} Pa) averaged over 55°E-65°E for days -3, 0, and +3.

GFDL CM2.1
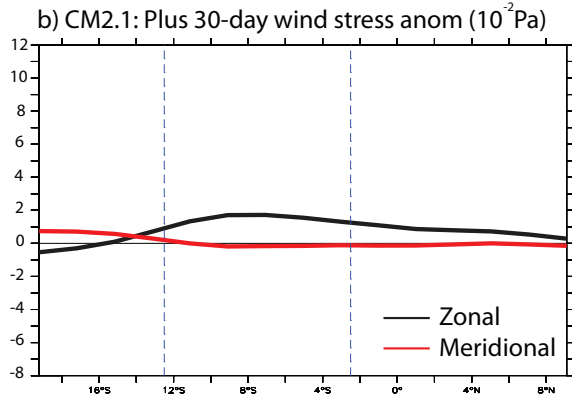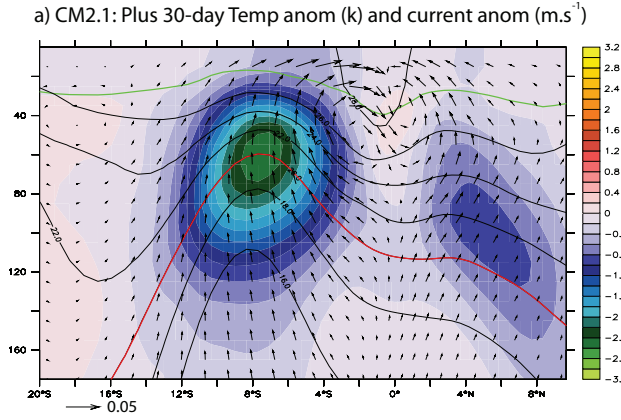
GFDL CM2.4
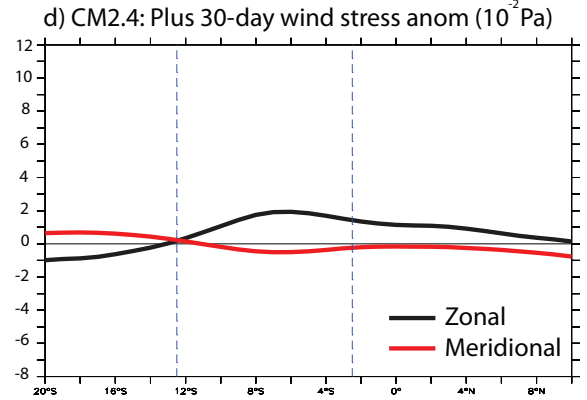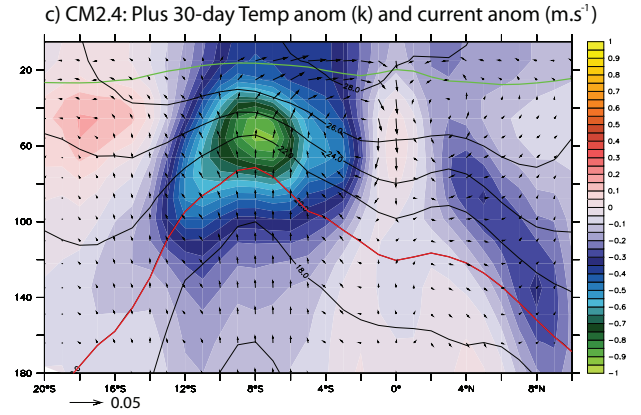
FIG. 6. a) GFDL CM2.1: Meridional cross section (55°E-65°E average) for the TRI composite on day 0. Shading indicates plus 30-day temperature anomaly (K); contours indicate mean temperature (K), with the red contour showing the 20K isotherm; arrows indicate plus 30-day current anomalies (m s^{-1}). The vertical scale for current anomalies is magnified by a factor of 10,000. b): GFDL CM2.1: Plus 30-day zonal wind stress anomaly (10^{-2} Pa) on day 0, averaged over 55°E-65°E. c) and d): Same as a) and b) respectively, but for GFDL CM2.4.
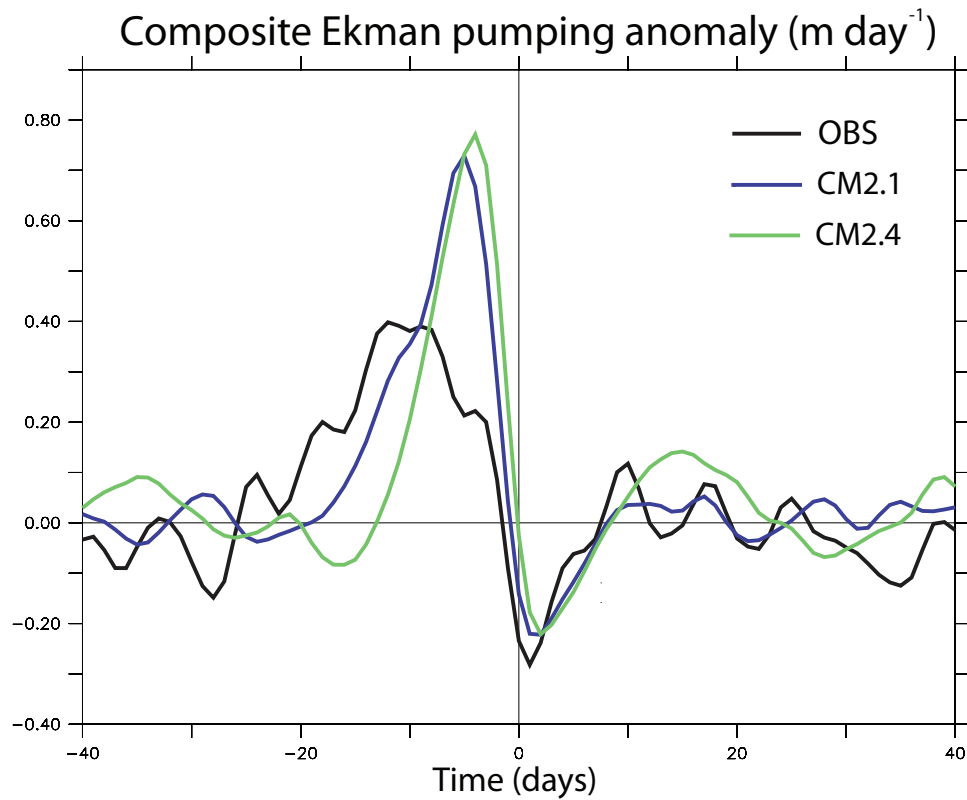
FIG. 7. Composite Ekman pumping anomaly (meters per day) for the TRI, calculated from Equation 9, for observations, GFDL CM2.1, and GFDL CM2.4.
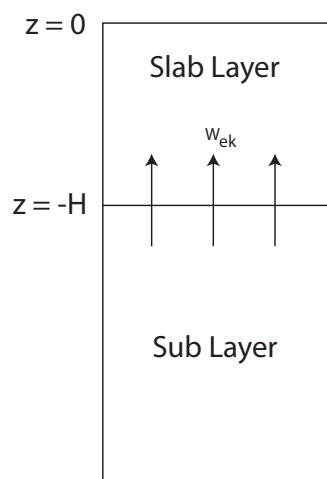
FIG. 8. Schematic of two-layer ocean approximation, for the Ekman upwelling argument in Section 3.c. w_{ek} represents the Ekman velocity at the depth $z = -H$, which is related to the wind stress curl.
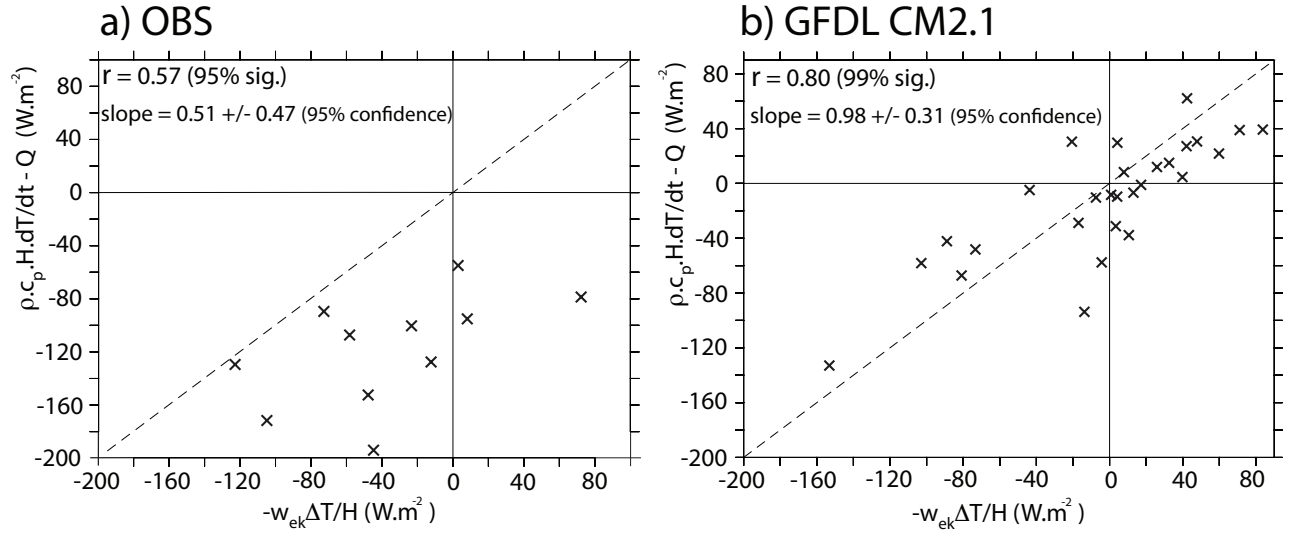
FIG. 9. a) Observations: Plot of LHS (y-axis) versus RHS (x-axis) from Equation 8, for a 15 day average prior to the minimum SST anomaly. Units are in W m^{-2}. The temperature anomaly in the slab layer is approximated by SST. b) GFDL CM2.1: Plot of LHS (y-axis) versus RHS (x-axis) from Equation 8, for a 15 day average prior to minimum SST anomaly (W m^{-2}).

a) CM2.1 preconditioning

b) CM2.4 preconditioning
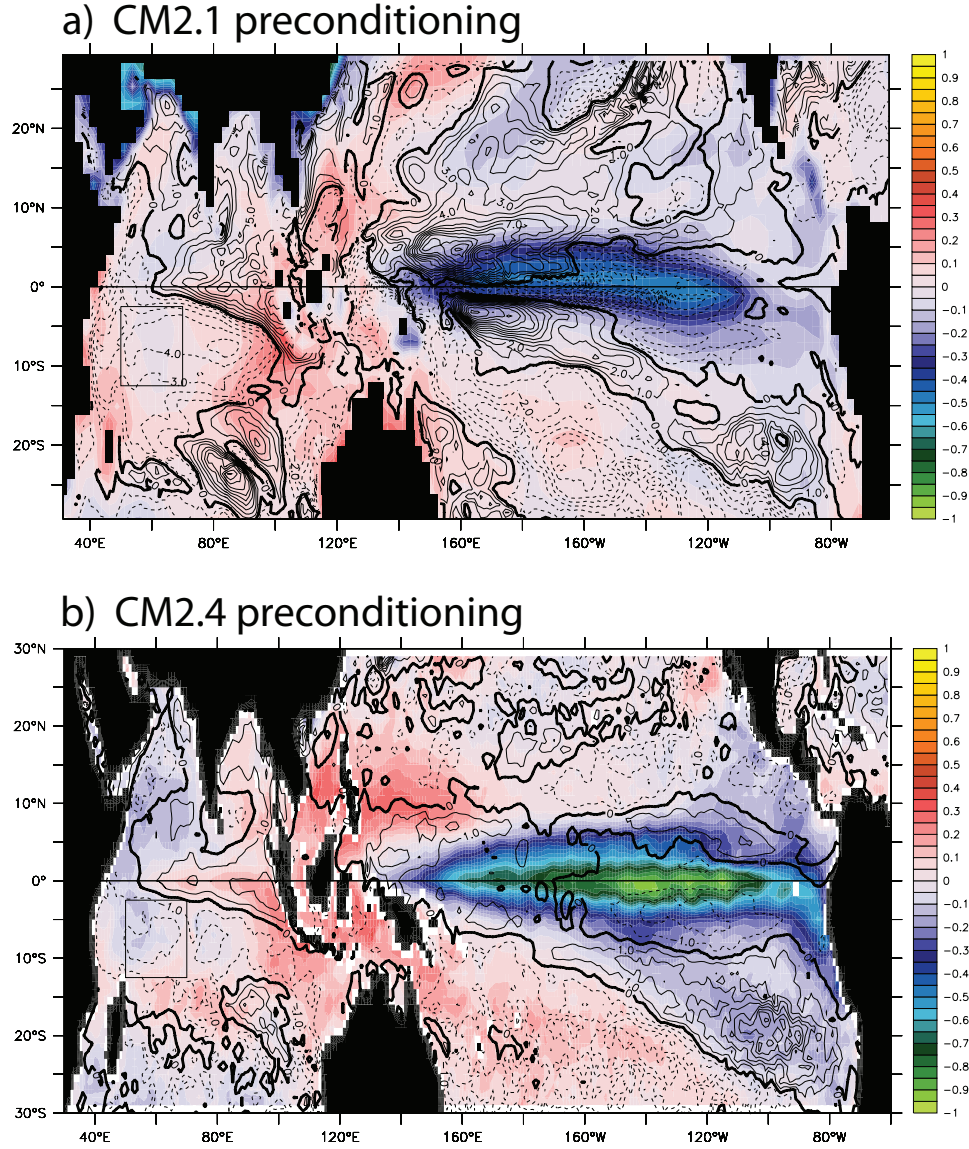
FIG. 10. Preconditioning for a) GFDL CM2.1 and b) GFDL CM2.4, for 5-12 weeks before cooling events occur, for the TRI composite. Shaded: SST anomaly (K); Contour: Mixed layer depth anomaly (m).
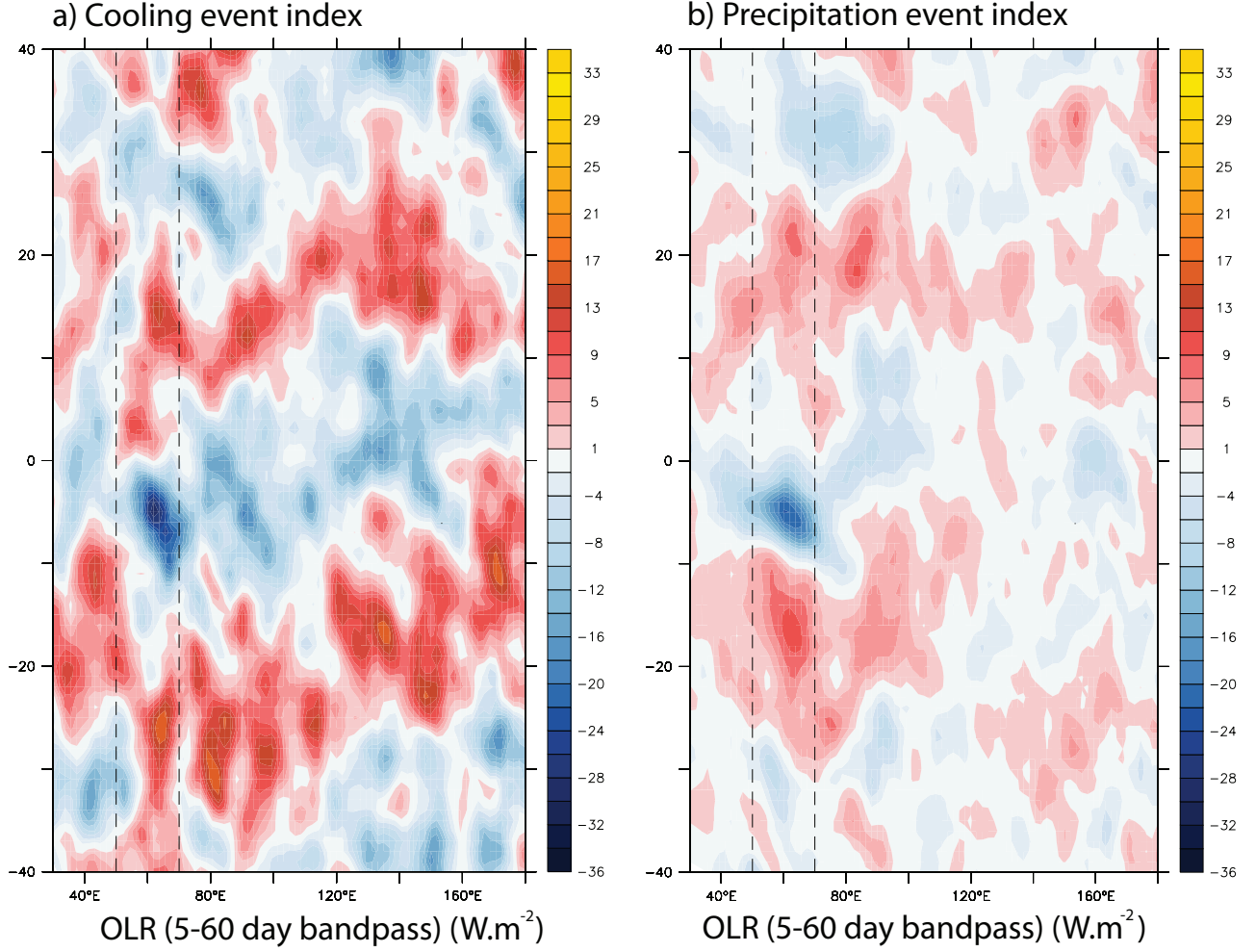
FIG. 11. a) Observations: Hovmoller diagram of OLR (W m^{-2}), based on the cooling event index, averaged over 5°S-12°S. The TRI is indicated by the dashed lines, with the SST anomaly minimum on day 0. Eastward propagation is present at approximately 5m s^{-1}. b) Observations: Hovmoller diagram of OLR (W m^{-2}), based on a precipitation event index, for precipitation events of 4 mm day^{-1} or more in the TRI (see Figure 12).
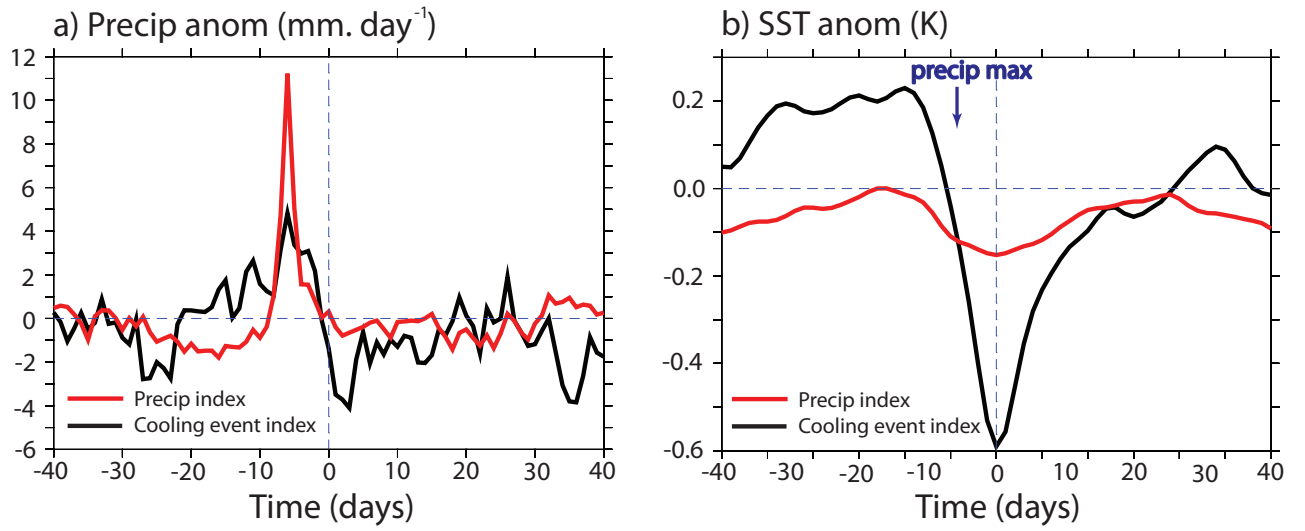
FIG. 12. a) Observations: Precipitation anomaly composite for both cooling event (black) and precipitation event (red) indices. b) Observations: Plot of SST anomaly (K) associated with cooling event index (black) and precipitation index (red).
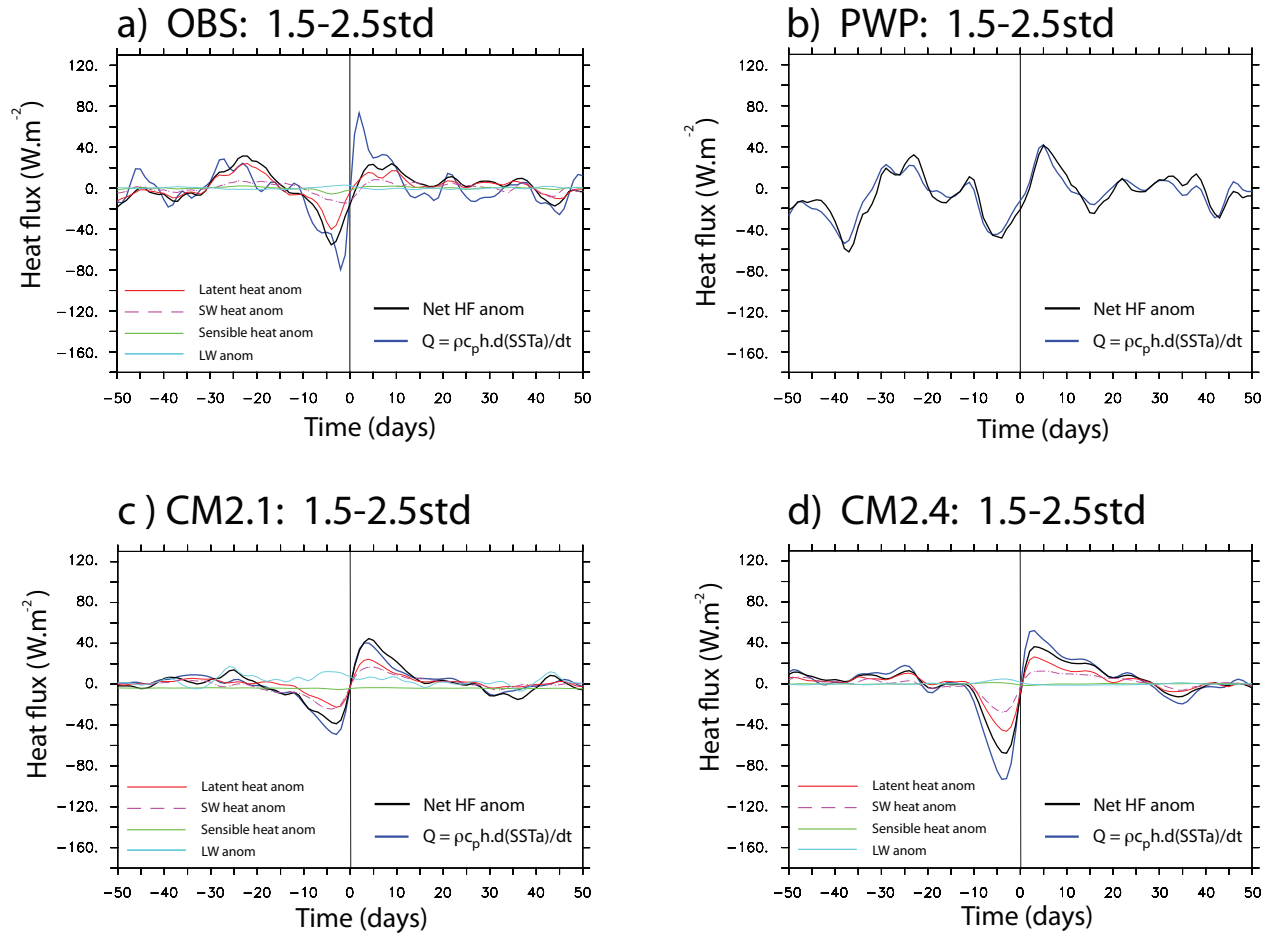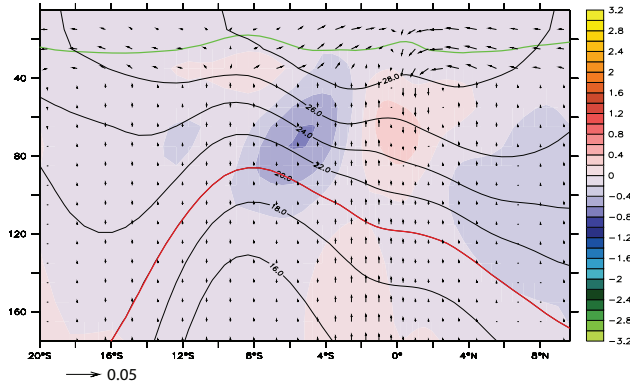
FIG. 13. Same as Figure 4, but using a 1.5 - 2.5σ criteria to calculate cooling event composites.

GFDL CM2.1: 1.5-2.5std

a) CM2.1: Plus 30-day Temp anom (k) and current anom (m.s^{-1})

GFDL CM2.4: 1.5-2.5std

c) CM2.4: Plus 30-day Temp anom (k) and current anom (m.s^{-1})
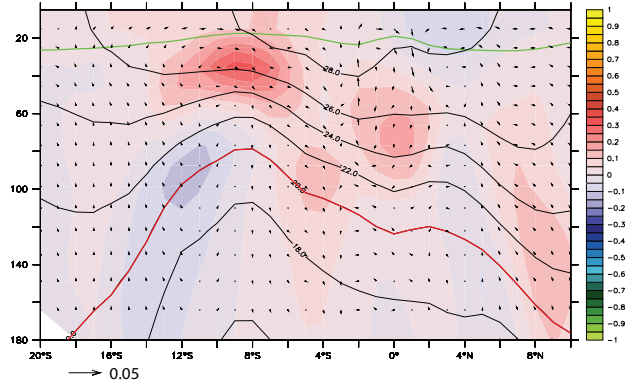

FIG. 14. Same as Figure 6.a and 6c, but using a 1.5 - 2.5σ criteria to calculate cooling event composites.
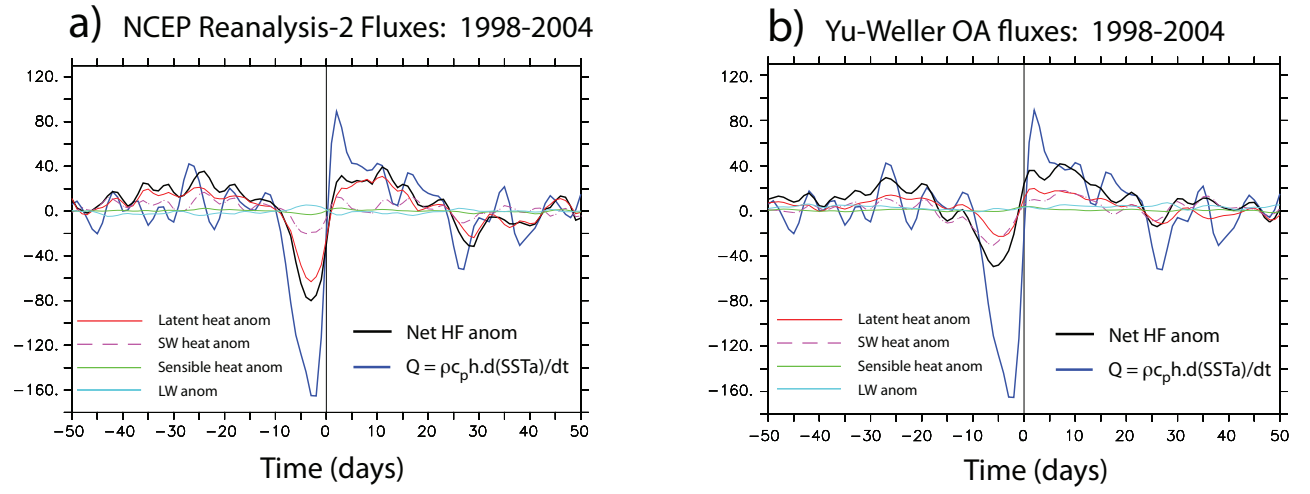
FIG. 15. Comparison of the slab model approach for a cooling event composite over the period 1998-2004 for a) NCEP Reanalysis-2 data and b) Yu-Weller flux data. Anomalies were calculated using monthly climatology for the period 1998-2007.